Supporting Information

Lin et al. 10.1073/pnas.1406391111

SI Text

Numerical Evaluation of the Critical Stress

Using the extremal dynamics protocol, the system evolves to the critical point with an average stress $\langle\Sigma_c(L)\rangle$ and stress fluctuations $\delta\Sigma$ in the stationary state with a dependence of system size as Eq. **13** in the main text. In Fig. S1 *Insets*, we plot out the $\langle\Sigma_c(L)\rangle$ as a function of $\delta\Sigma(L)$, and the critical stress in the thermodynamic limit is just the intersection of the curves with the y-axis, and we get $\Sigma_c = 0.5221 \pm 0.0001$ for dimension $(d) = 2$ and $\Sigma_c = 0.5058 \pm 0.0002$ for $d = 3$. From the dependence of $\delta\Sigma$ on L, shown in Fig. S1, we also extract $\nu = 1.16 \pm 0.04$ in $2d$ and $\nu = 0.72 \pm 0.04$ in $3d$.

Fixed-Stress Protocol

At fixed stress in a finite size system, the dynamics eventually will stop. To trigger a new avalanche, we give random kicks to all sites, of amplitude δx_j, while keeping Σ fixed. We consider two methods. In the first one, a site i is chosen randomly, and the amplitude of the kicks follows:

$$\delta x_j = -A\mathcal{G}(\vec{r}_{ij}), \qquad [\text{S1}]$$

where A is a constant adjusting the amplitude of kicks. Data presented in the text correspond to $A = 1$, but choosing smaller values of A, such as 0.1 did not affect the results (see Fig. S4). Eq. **S1** ensures that the stress is constant. If no sites become unstable, another site is chosen randomly and another set of kicks following Eq. **S1** is given. In this method, the site j_0 that eventually becomes unstable typically was close to an instability before the random kicks were given. However, j_0 is not necessarily the weakest site in the entire system.

In the second method, the dynamics are triggered by imposing that the weakest site o (i.e., $x_o < x_i$ for all $i \neq o$) yields. According to our automaton model, this leads to a change of local distance to instability everywhere in the system, which follows

$$\delta x_j = -\mathcal{G}(\vec{r}_{oj}) \qquad [\text{S2}]$$

and may lead to avalanches. We find that these two methods give consistent results for τ, as shown in Fig. S4.

Finite Size Collapse of the Flow Curve

Our estimations of the threshold Σ_c and the correlation length exponent ν are obtained in the main text by using the extremal dynamics protocol. We obtain the same results if we use the fixed-stress protocol, with which we can compute the size-dependent flow curve relating the strain rate, $\dot{\gamma}$, as a function of the external stress, Σ. From general arguments of finite size scaling, we expect

$$\dot{\gamma} \sim L^{-\beta/\nu} f\left((\Sigma - \Sigma_c)L^{1/\nu}\right). \qquad [\text{S3}]$$

To test the consistency of our methods, in Fig. S2 we collapse the different flow curves using Eq. **S3** and the value of Σ_c, ν, and β initially obtained with the extremal dynamics protocol. We observe a satisfying collapse without any free parameter.

Avalanche Statistics

To extract the avalanche distribution exponent τ accurately, we compare two protocols: (*i*) constant stress at Σ_c and (*ii*) extremal dynamics, as shown in Fig. S3. It turns out that the avalanche distributions in extremal dynamics have stronger finite size effects than at constant stress. It thus is difficult to extract the avalanche exponent τ accurately by using extremal dynamics. From Fig. S3, *Right*, *Inset*, τ does not change significantly with system size in the constant-stress method, in contrast to the estimate of τ that increases with L in extremal dynamics. To extract τ accurately, we fix the stress at Σ_c to collect the avalanche statistics, and we find $\tau = 1.36 \pm 0.03$ in $2d$, and $\tau = 1.45 \pm 0.05$ in $3d$, and the value of τ is the same for the two methods of fixed-stress protocol, and also insensitive to the value of A in the first method, shown in Fig. S4. The error associated with the exponent is estimated by varying the range of avalanche sizes considered in the fit.

General Scaling Relations

The three scaling relations derived in the main text for the critical exponents of the yielding transition are similar but not identical to the scaling relations obtained for the depinning transition of an elastic interface. In the following, we derive three more general relations, namely

$$\nu = \frac{1}{d - d_f + \alpha_k} \qquad [\text{S4}]$$

$$\beta = \nu(d - d_f + z) \qquad [\text{S5}]$$

$$\tau = 2 - \frac{d_f - d + 1/\nu}{d_f} - \frac{\theta}{\theta + 1}\frac{d}{d_f}, \qquad [\text{S6}]$$

that hold both for yielding and depinning. Here, α_k is the dimension of the interaction kernel $\mathcal{G}$. In the context of the yielding transition, $\alpha_k = 0$ and $d_f < d$ so that $\beta > 1$. In the context of the depinning transition $\theta = 0$ and $d_f \geq d$, the dimension of the interaction kernel is $\alpha_k = 2$ for the short-range elasticity and $\alpha_k = 1$ for the long-range elasticity of the contact line of a liquid meniscus (1) or of the crack front in brittle materials (2, 3).

Note that relations **S5** and **S6** are expected to be very general, whereas the first relation is guaranteed only in the presence of statistical tilt symmetry, hence only when the interactions are linear. For example, it is known that the nonharmonic corrections to the elastic energy can modify the universal behavior of the depinning transition with critical exponents that violate relation **S4** (4). For the yielding transition, the validity of **[S4]** is supported by recent molecular dynamics simulations (5) that show that the stress decay during an avalanche is proportional to the energy jump, a scaling consistent with linear elasticity. Such linearity is assumed a priori in elasto-plastic models and is required for the statistical tilt symmetry to apply (see below).

From the Elasto-Plastic Automaton to the Continuum Model. The d dimensional elasto-plastic model studied in this paper is a discrete automaton. Its continuum limit gives the time evolution of the strain field $\gamma_{\vec{r}}$ in each point of the space:

$$\partial_t \gamma_{\vec{r}} = \int_{\vec{r}'} \mathcal{G}(\vec{r} - \vec{r}')\gamma_{\vec{r}'} + \Sigma + \sigma^{\text{dis}}(\gamma_{\vec{r}}, \vec{r}). \qquad [\text{S7}]$$

The first term of the equation describes the interactions between the different parts of the system. Note that the interactions are

linear in the strain field γ, and governed by a time-independent interaction kernel, $\mathcal{G}(\vec{r})$. As discussed in the main text, for elastic depinning models the kernel is monotonic, whereas for amorphous materials it is nonmonotonic, anisotropic and may be conveniently written in the Fourier space:

$$\mathcal{G}(\vec{k}) = \begin{cases} -\dfrac{4k_x^2 k_y^2}{k^4}, & \text{for } d=2 \\[2mm] -\dfrac{4k_x^2 k_y^2 + k_z^2 k^2}{k^4}, & \text{for } d=3. \end{cases} \quad \text{[S8]}$$

The other two terms are the external stress, Σ, and the quenched disorder, $\sigma^{\text{dis}}(\gamma, \vec{r})$, which takes into account the inhomogeneities of the local yield stress. In the automaton model, the scalar stress σ_i corresponds to the sum of the first two terms, and $\sigma^{\text{dis}}(\gamma, \vec{r})$ is assumed to be a collection of narrow wells randomly located along $\vec{r}$. The parameters σ^{th}, ε, and τ_c are related, respectively, to the well depth, the distance between consecutive wells, and the time needed to move from an unstable well to a stable one.

Below threshold, $\Sigma < \Sigma_c$, the local strain fields are pinned inside a set of narrow wells. If a small perturbation is applied (e.g., a little change in the well locations), the local strain field responds either (almost everywhere) linearly simply by readjusting its value inside the well or (when a well becomes unstable) with a large modification accompanied by a stress release that may be the seed of a large avalanche. This nonlinear response gives a singular contribution to the susceptibility, which becomes important close to Σ_c. Note that in the presence of a nonmonotonic interaction kernel, the avalanche size $S = \sum_i \Delta \gamma_i$ may be positive or negative; however, the positive external stress Σ strongly suppresses negative avalanches that, in practice, may be neglected.

The Statistical Tilt Symmetry. We now focus on the response of the system when we add to Eq. **S7** a tilt, $\sigma_{\vec{r}}^{\text{tilt}}$, namely an inhomogeneous local stress of zero spatial average. In the presence of linear interactions, the tilt can be absorbed in a new strain field $\tilde{\gamma}_r$ defined as

$$\tilde{\gamma}_{\vec{r}} = \gamma_{\vec{r}} + \int_{\vec{r}'} \mathcal{G}^{-1}(\vec{r} - \vec{r}') \sigma_{\vec{r}'}^{\text{tilt}} \quad \text{[S9]}$$

and governed by the following evolution equation:

$$\partial_t \tilde{\gamma}_r = \int_{\vec{r}'} \mathcal{G}(\vec{r} - \vec{r}') \tilde{\gamma}_{\vec{r}'} + \Sigma + \sigma^{\text{dis}}(\tilde{\gamma} - \mathcal{G}^{-1}\sigma^{\text{tilt}}, \vec{r}). \quad \text{[S10]}$$

The latter equation points out that the effect of the tilt may be absorbed with a shift in the location of the narrow wells. Thus, once the average over disorder is taken, the tilt disappears from Eq. **S10** if the correlation $\overline{\sigma^{\text{dis}}(\gamma, \vec{r})\sigma^{\text{dis}}(\gamma', \vec{r}')}$ depends only on $\gamma - \gamma'$. For example, in the steady state, when the system becomes independent of the initial conditions, the average response of γ_q to a tilt σ_q^{tilt} acting on the mode q, is

$$\chi_q = \frac{\overline{\partial \gamma_q}}{\partial \sigma_q^{\text{tilt}}} = \frac{\overline{\partial \tilde{\gamma}_q - \mathcal{G}_q^{-1}\sigma_q^{\text{tilt}}}}{\partial \sigma_q^{\text{tilt}}} = -\mathcal{G}_q^{-1}. \quad \text{[S11]}$$

This exact expression should be compared with the scaling behavior of the singular part of the susceptibility governed by the characteristic scale $\xi \sim (\Sigma_c - \Sigma)^{-\nu}$. In this regime, the strain field grows as $\Delta \gamma \simeq \xi^{d_f - d}$ and noting that the tilt has the dimension of a stress, we expect that the singular part of the susceptibility scales as $\chi^{\text{sing.}} \sim \xi^{1/\nu + d_f - d}$, which gives $1/\nu - d + d_f = \alpha_k$, namely Eq. **S4**. Here, α_k is the dimension of the kernel $1/\mathcal{G}_q$. For short-range elastic depinning, $\alpha_k = 2$, and for long-range depinning, $\alpha_k = 1$, whereas the anisotropic kernel one has $\alpha_k = 0$.

Stationarity. Concerning the other two scaling relations: Eq. **S5** is identical to the one derived in the main text and Eq. **S6** is still a consequence of the stationarity of the avalanche dynamics. In general, an avalanche of size S leads to a stress drop that is not simply proportional to the plastic strain, but rather to $\Delta \gamma L^{d - d_f - 1/\nu}$, so that the average stress drop induced by avalanches scales as

$$\Delta \Sigma \sim \frac{\langle S \rangle}{L^d} \frac{L^{-1/\nu}}{L^{d_f - d}}. \quad \text{[S12]}$$

On the other hand, the stress injection before a new avalanche is observed scales as $L^{-d/(\theta+1)}$, so that

$$\frac{\langle S \rangle}{L^d} \frac{L^{-1/\nu}}{L^{d_f - d}} \sim L^{-d/(\theta+1)}. \quad \text{[S13]}$$

Finally, using $\langle S \rangle \sim L^{(2-\tau)d_f}$, we obtain Eq. **S6**.

1. Joanny JF, De Gennes PG (1984) A model for contact angle hysteresis. *J Chem Phys* 81:552.
2. Gao H, Rice JR (1989) A first-order perturbation analysis of crack trapping by arrays of obstacles. *J Appl Mech* 56:828.
3. Bonamy D, Bouchaud E (2011) Failure of heterogeneous materials: A dynamic phase transition? *Phys Rep* 498(1):1–44.

4. Kardar M (1998) Nonequilibrium dynamics of interfaces and lines. *Phys Rep* 301(1): 85–112.
5. Salerno KM, Robbins MO (2013) Effect of inertia on sheared disordered solids: Critical scaling of avalanches in two and three dimensions. *Phys Rev E Stat Nonlin Soft Matter Phys* 88(6):062206.
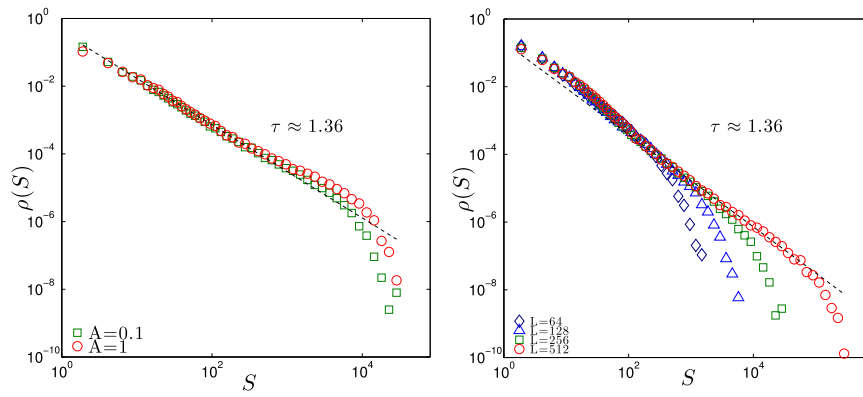
Fig. S1. Stress fluctuations for the extremal dynamics simulation, from which we extract the correlation length exponents $\nu = 1.16 \pm 0.04$ in $2d$, and $\nu = 0.72 \pm 0.04$ in $3d$. (*Insets*) The relation between $\Sigma_c(L)$ and $\delta\Sigma$. The intersection of the curves with the y-axis yields Σ_c in the thermodynamic limit.

Fig. S2. Collapse of the flow curves obtained from Eq. **S3** using the estimations of β, Σ_c, and ν given in Table 2 of the main text for $d = 2$ (*Left*) and $d = 3$ (*Right*).

Fig. S3. (*Left*) Avalanche distributions at Σ_c in $2d$. These distributions clearly overlap for a range of sizes growing with L. In this range, we obtain an exponent $\tau = 1.36 \pm 0.03$. Here $A = 1$; we check the distributions with a much gentler $A = 0.1$ and find the same τ. (*Inset*) Avalanche distribution in $3d$ leading to $\tau = 1.45 \pm 0.05$ for $L = 64$. (*Right*) Avalanche distribution obtained by using extremal dynamics with the same three sizes. These distributions do not clearly overlap, leading to exponents apparently increasing with system size. (*Inset*) How τ changes with size by using these two different methods.

Fig. S4. (*Left*) Effect of the magnitude of random kicks *A* on the estimation of τ for the first method of fixed-stress simulation, for *L* = 256 and *d* = 2. (*Right*) Normalized avalanche probability distribution extracted using the second method of fixed-stress simulation (for which the weakest site yields). This method yields the same exponent τ = 1.36.